Advances in Aircraft and Spacecraft Science, *Vol. 13, No. 1 (2026) 1-15*
https://doi.org/10.12989/aas.2026.13.1.001

Techno-Press

Numerical study of the fracture behavior of single-lap joints with bi-adhesive in shear tests

Mohammed C. Ezzine*[1,2], Ilias M.A. Ghermaoui[2],
Kawther F.Z. Ezzine[3], Mohamed Mokhtari[4]

[1]*Department of Mechanical Engineering, Mustapha Stambouli University of Mascara, 29000 Mascara, Algeria*
[2]*Laboratoire Mécanique Physique des Matériaux, Department of Mechanical, Djillali Liabes University 22000 Sidi Bel Abbes, Algeria*
[3]*Department of physics, Faculty of Exact Sciences, Djillali Liabes University 22000 Sidi Bel Abbes, Algeria*
[4]*Laboratoire LaRTFM, Ecole Nationale Polytechnique Maurice Audin, 31000 Oran, Algeria*

(Received October 25, 2025, Revised January 26, 2026, Accepted January 30, 2026)

Abstract. One of the primary causes of a decrease in strength in adhesive joints is the presence of stress concentrations at the ends of the overlap region. To address this issue effectively, the bi-adhesive technique has been introduced to minimize stress concentrations at the overlap ends. Several research efforts have been devoted to studying single lap adhesive joints. However, this type of assembly exhibits stress concentrations at the ends of the joint, in contrast to its inactive core. The aim of this research is to present a numerical analysis of single lap bi-adhesive joints using cohesive zone models with four different adhesives. Two adhesives of the same chemical composition, one rigid and one flexible, were used. The overlap length parameters for each adhesive area were considered. Thus, the placement of both rigid and flexible adhesives was optimized. The combination of both adhesives in a single lap adhesive joint, with the more rigid adhesive positioned at the core of the joint, provided enhanced strength to the assembly with a 37% improvement. The variation in overlap length of the adhesives in the bi-adhesive joints affected the joint toughness. Among them, the best results were obtained when covering 40% to 60% of the overlap length with the more rigid adhesive at the core of the joint.

Keywords: bi-adhesive joint; cohesive zone models; failure; single lap joint

1. Introduction

Bonded structures have been widely used in the automotive, electronics, aerospace, and other fields due to their advantages of uniform stress distribution, high strength-to-weight ratio, and good damage and corrosion resistance [1], [2]. Adhesively bonded joints can improve stiffness and enhance the uniformity of the stress field in the bonded joint, thereby relieving stress concentrations and ensuring high fatigue resistance compared to welding, riveting, and bolted joints. The mechanical properties and adhesive strength under shear conditions are commonly evaluated through extensive research on the single-lap joint, which is considered the most extensively studied type of bonded joint. This choice is driven by its straightforward geometry and ease of implementation.

*Corresponding author, Ph.D., E-mail: ezzine_chamseddine@yahoo.fr

Copyright © 2026 Techno-Press
http://www.techno-press.org/aas/5
ISSN: 2287-528X (Print), 2287-5271 (Online)

The finite element method has been widely used to predict the behavior of bonded joints [3]. Stress concentrations at the ends of bonded joints can significantly reduce bond strength and result in the premature failure of adhesive joints. Several studies have proposed various methods to reduce stress concentrations at the ends of adhesive joints, such as modifying geometrical dimensions, enhancing the mechanical properties of the adhesive, in particular, by incorporating nanoparticles to increase toughness and mitigate stress concentrations in critical regions, thinning the substrates, or even applying chamfers [4]. However, each method presents its own limitations.

Ozer and Oz [5] proposed a three-dimensional model for a bi-adhesive double-lap joint, employing solid and contact elements to investigate the influence of bondline configuration on stress distribution. L.F.Da Silva and M.J.Lopes [6] proposed that an optimal adhesive joint can be achieved by varying the flexibility and strength properties along the bonded overlap. Pires et al. [7] examined the failure mechanisms associated with bi-adhesive joints and reported a notable improvement in shear strength compared to joints bonded entirely with a single adhesive. Their findings indicated that this enhancement in lap-shear performance could be accurately predicted through finite element modelling. Oz and Ozer [8] investigated the influence of bi-adhesive bondline configurations on von Mises stress distribution. Their study involved both analytical and numerical analyses conducted across three distinct bi-adhesive layouts. The results revealed a significant reduction in peak von Mises stress in the bi-adhesive joints compared to those utilizing a single adhesive along the entire bondline.

The pursuit of joints with high shear strength and substantial failure loads has led to the use of rigid adhesives [9], [10]. However, these adhesives exhibit pronounced stress concentrations at the bond ends, which may result in low failure loads. Conversely, according to Volkersen's theory [11], the use of lower stiffness adhesives enhances joint strength by reducing stress concentrations at the bond ends and promoting a more uniform stress distribution. Nevertheless, adhesives with higher shear strength remain necessary to avoid sudden shear failure.

Strength prediction of single-lap joints (SLJs) initially relied on analytical approaches, assuming that stress transfer occurs only through shear stresses in the adhesive, while the adherends are subjected solely to normal stresses [12]. Subsequently, the strength and behavior of SLJs with similar and dissimilar adherends were investigated experimentally and numerically under various loading conditions [13-16].

Cohesive zone models (CZMs) have been widely used to predict the strength of adhesive joints [17-20]. These models complement finite element analysis by enabling the simulation of damage initiation and propagation in materials or at interfaces between different materials [21], [22], and are commonly employed to model delamination at the substrate–adhesive interface in bonded joints [23], [24]. Ezzine et al. [25] developed a cohesive-element-based model validated using Double Cantilever Beam (DCB) and End-Notched Flexure (ENF) tests, which was subsequently applied to single-lap joints. In fracture-based analyses, it is essential to determine the critical energy release rates in mode I (G_{IC}) and mode II (G_{IIC}) [26-28]. In addition, the cohesive strengths in tension (t_{n0}) and shear (t_{s0}) must be identified, particularly at the onset of damage.

This study aims to enhance bonded joint performance using a bi-adhesive configuration. FEM with CZM is employed to investigate failure behavior and crack propagation under shear loading. The CZM is used to model crack propagation in bonded joints through a bilinear traction–separation law implemented in the ABAQUS finite element software. After validating the numerical model against experimental data obtained with the epoxy adhesive Adekit A140, additional simulations were performed using adhesives of varying stiffness, including Araldite AV138, Araldite 2015, and Sikaforce 7752. Following this validation, bi-adhesive joints

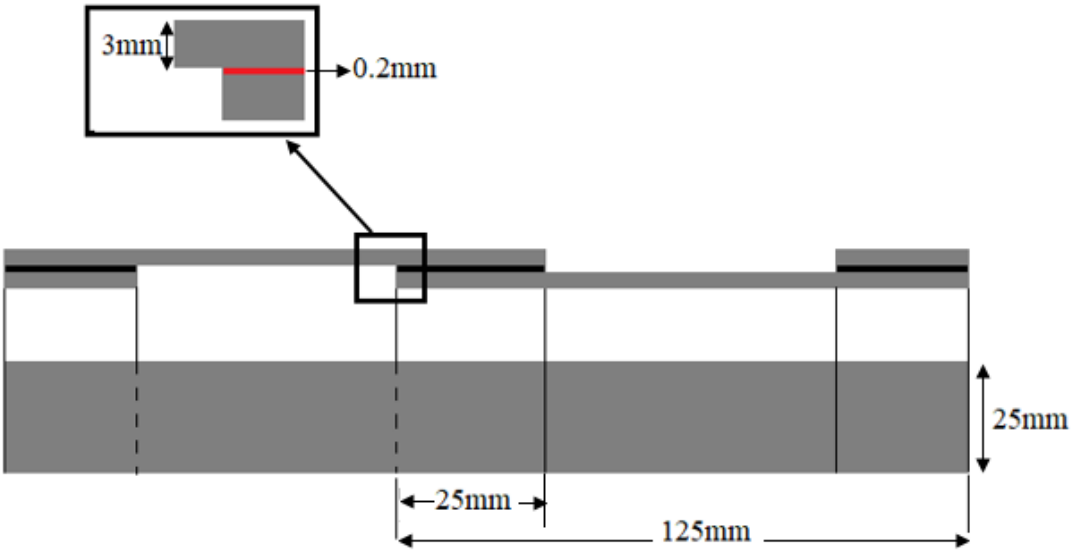

Figure 1. Schematic design of a single lap joint

combining two adhesives from the same chemical family (Araldite AV138 and Araldite 2015) were analyzed with varying overlap lengths to assess their effectiveness in improving joint performance and overall assembly strength.

2. Geometric model description

A three-dimensional model is selected to analyze single-lap bonded joints with dimensions ($125 \times 25 \times 3$ mm³), assembled using a bonding process with four different adhesives. Fig. 1 illustrates the joint geometry. Shims are placed at the ends to maintain the symmetry of the applied forces in the plane of the bonded joint.

3. Mechanicals properties

The assembled plates are made of E24 steel, whose mechanical properties are shown in Table 1:

Table 1. Mechanical properties of steel E24 plate [25]

Properties	Values
Young's modulus [Gpa]	205
Tensile strength [Mpa]	11.1
Yield strength [Mpa]	7.1
Shear modulus [Gpa]	80
Poisson's ratio	0.32

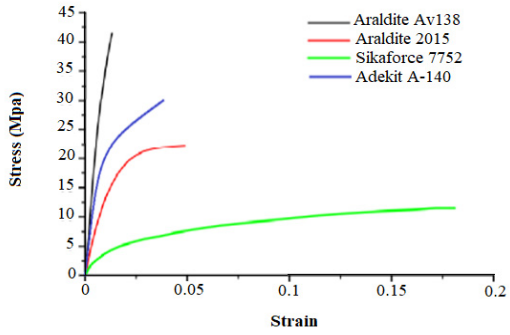

Figure 2. Tensile stress–strain curves of the analyzed adhesives [25], [27]

Table 2. Mechanical properties of Araldite AV138, Araldite 2015, Sikaforce 7752, and Adekit A140 adhesives [25], [27]

Properties	Araldite AV138	Araldite 2015	Sikaforce 7752	Adekit A140
Young's modulus (GPa)	4.89 ± 0.81	1.85 ± 0.21	0.49 ± 0.09	2.66
Poisson's ratio	0.35	0.33	0.30	0.35
Tensile yield stress (MPa)	36.49 ± 2.47	12.63 ± 0.61	3.24 ± 0.48	7.02
Tensile strength (MPa)	39.45 ± 3.18	21.63 ± 1.61	11.48 ± 0.25	30
Shear modulus (GPa)	1.56 ± 0.01	0.56 ± 0.21	0.19 ± 0.01	0.985
Shear strength (MPa)	30.2 ± 0.40	17.9 ± 1.8	10.17 ± 0.64	35.9
Toughness in tension, G_{IC} (N/mm)	0.20	0.43 ± 0.02	2.36 ± 0.17	0.5
Toughness in shear, G_{IIC} (N/mm)	0.38	4.70 ± 0.34	5.41 ± 0.47	2.41

In order to study the effect of interface properties on the bonding process and the failure behavior of the plate/adhesive/plate assembly, four adhesives were selected to predict joint detachment: Adekit A140, Araldite AV138, Araldite 2015, and Sikaforce 7752 (Table 2, Fig. 2).

The adhesives Araldite AV138 and Araldite 2015 exhibit significantly different behaviors, with the former being more resistant than the latter; however, its viscoplastic behavior is less pronounced. Sikaforce 7752, on the other hand, exhibits a fully viscoplastic behavior (Fig. 2). Adekit A140 demonstrates an intermediate behavior among these four adhesives. To model adhesive joint damage, it is essential to consider the failure parameters of these adhesives (Table 2).

4. Numerical study

A three-dimensional (3D) finite element model was established within the ABAQUS environment to study the behavior of the joint. The types of elements used in this study are as

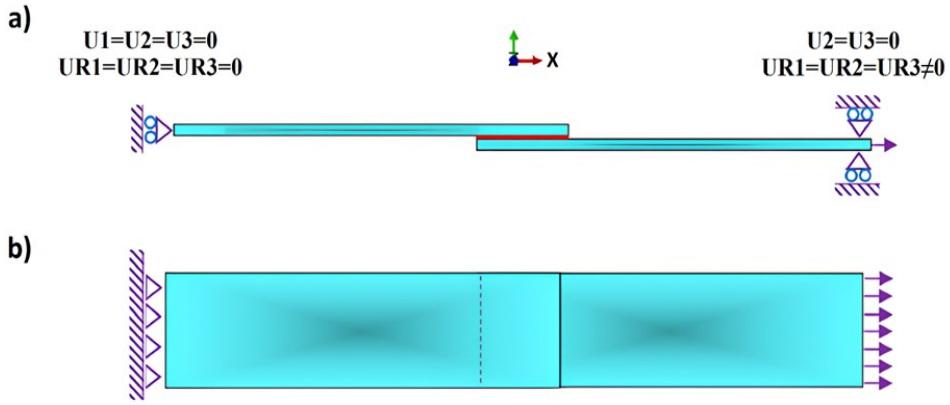

Figure 3. Single lap joint geometry with the boundary condition. In (a) side view and (b) plan view

follows: 8-node brick elements (C3D8R) with reduced integration were employed to model the steel plates. Additionally, typical COH3D8 elements were used to model the adhesive interface, the cohesive zone is defined by cohesive elements where the crack growth will occur. A bilinear traction–separation law was selected to model the behavior of the adhesive–substrate interfaces. The model was partitioned to allow mesh refinement in the bonded region. Cohesive elements with a size of 0.2 mm² were used in this area, resulting in a total of 3125 cohesive elements. The overall model comprises 11250 elements. The simulations were carried out using the explicit version of the ABAQUS finite element code, incorporating Arbitrary Lagrangian–Eulerian (ALE) adaptive meshing. The parameters for the adhesive's cohesive models, including the critical energy release rates in mode I (G_{IC}) and mode II (G_{IIC}), as well as the cohesive strengths in tension (t_n) and shear (t_s), were obtained from Table 2. The boundary conditions applied to the numerical models are illustrated in Fig. 3, where the degrees of freedom (DOFs) are explicitly indicated. At the fixed end of the joint, all translational and rotational degrees of freedom are constrained (U1=U2=U3=0, and UR1=UR2=UR3=0) At the loaded end, the transverse and out-of-plane displacements are constrained (U2=U3=0), while a prescribed displacement is applied in the longitudinal direction (U1≠0). The rotational degrees of freedom at the loaded end are left free (UR1=UR2=UR3≠0) in order to avoid artificial bending constraints and to better reproduce the experimental loading conditions.

4.1 Cohesive zone model

A cohesive zone model is used to analyze crack propagation. The cohesive zone is defined by cohesive elements or by the intersection of occurring cracks. The cohesive law selected to model the behavior of the adhesive/substrate interfaces is a bilinear traction-separation law proposed by P.P.Camanho and C.G.DAVILA [29]. The tensile or shear stress ($ti,\ i = n;\ t$) at the interface increases linearly with the opening δi, at a slope defined by the parameter K, which represents the initial stiffness of the cohesive zone. When the critical stress $ti,\ max$ is reached, the interface begins to degrade. Eventually, the opening between the two lips of the interface reaches a critical value $\delta i,m$ corresponding to interface failure (Fig. 4). The traction-separation relationship can be expressed as Eq. (1)

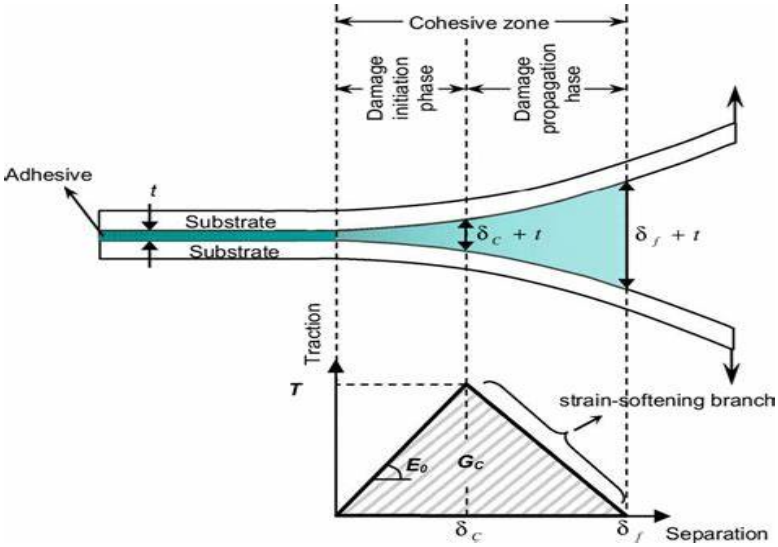

Figure 4. Schematic damage process zone and corresponding bi-linear traction–separation law in an adhesively bonded joint [26]

$$t_i = \begin{cases} (1-D)K\delta i \\ D = \frac{\delta i,m}{\delta i,m-\delta i,0}\left(1-\frac{\delta i,0}{\delta i}\right) \quad \text{if} \delta i > \delta i,0 \text{ if not } D = 0, \\ D = \min(D,1) \end{cases} \tag{1}$$

The cohesive zone model (CZM) approach remains the most suitable method for describing adhesive damage. In this approach, the damage path is entirely contained within the cohesive zone (Fig. 4). The damage evolution model follows a linear traction-separation law (Fig. 3) and is defined at a nodal surface in the mesh where no interaction has been introduced between the surfaces. Indeed, the evolution of the damage is given according to the distance between the nodes until a critical length which corresponds to D=1.

4.1.1 Criterion for initiation of damage

A threshold stress for damage initiation is defined, leading to a softening behavior in which stiffness degradation increases as the surfaces separate. To model this process, the two surfaces reach a critical level of separation, causing the connecting stiffness to approach zero, ultimately resulting in complete detachment. The initiation of damage is characterized using a modified quadratic stress criterion (QUADS DAMAGE), which accounts for both the critical tensile stress $t_{n,max}$, and the critical shear stress $t_{s,max}$ [30]

$$\left(\frac{t_n}{t_{\text{n,max}}}\right)^2+\left(\frac{t_{s1}}{t_{\text{s,max}}}\right)^2+\left(\frac{t_{s2}}{t_{\text{s,max}}}\right)^2=1, \tag{2}$$

4.1.2 Criterion of damage propagation

The damage propagation law used in this study follows the Benzeggagh-Kenane (BK) rupture criterion [31]. This criterion defines crack propagation in mode I, mode II, and mixed-mode I/II (Fig. 5). It is formulated as a function of the energy release rate G

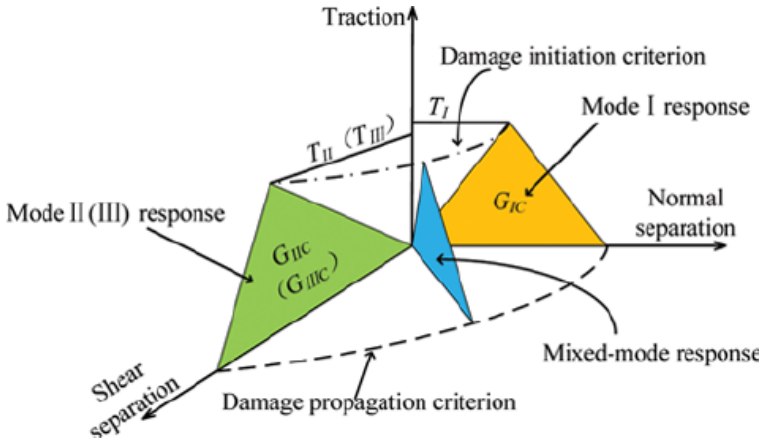

Figure 5. Mixed-mode triangle traction-separation law [19]

$$G_{IC}+(G_{IIC}+G_{IC})\left\{\frac{G_S}{G_T}\right\}^n = G_C. \quad (3)$$

Where $G_S = G_{II} + G_{III}$, $G_T = G_I + G_S$ and η is a characteristic material parameter, G_{ic} is the critical energy release rate associated with fracture mode i. (with i = I Mode I, i = II and i = III modes II and III respectively).

5. Results and discussion

5.1 Damage and failure of a single-lap joint with adhesive Adekit A140

A three-dimensional finite element (FE) model was established to validate the experimental results of the single-lap joint with Adekit A140. The cohesive zone at the substrate-adhesive interface is represented using cohesive elements (Fig. 6).

Fig. 6 illustrates the evolution of the von Mises stress distribution in the single-lap joint during damage progression at selected imposed displacements. Before damage (δ = 2.5 mm), stress concentrations are mainly located at the ends of the overlap, which is characteristic of single-lap joints, with a maximum von Mises stress of about 163 MPa. As the imposed displacement increases to δ = 2.85 mm, damage initiation occurs at these critical regions due to the progressive increase in stress levels, reaching a peak value of approximately 302 MPa. Further loading (δ = 3.3 mm) leads to damage evolution accompanied by crack propagation along the adhesive interface, resulting in a reduction of the maximum stress to about 103 MPa. The last displacement (δ = 4.0 mm) corresponds to the post-damage stage of the joint, where the stress level drops significantly to around 0.14 MPa, indicating joint failure. Overall, the results show that the von Mises stress increases up to damage initiation and then decreases progressively until complete failure.

Fig. 7 presents a comparison between experimental and numerical force–displacement curves for a single-lap joint using Adekit A140 adhesive. The results clearly demonstrate the effectiveness of the numerical model based on cohesive zone modeling, as an excellent agreement is observed between numerical predictions and experimental data reported by Ezzine et al. [25].

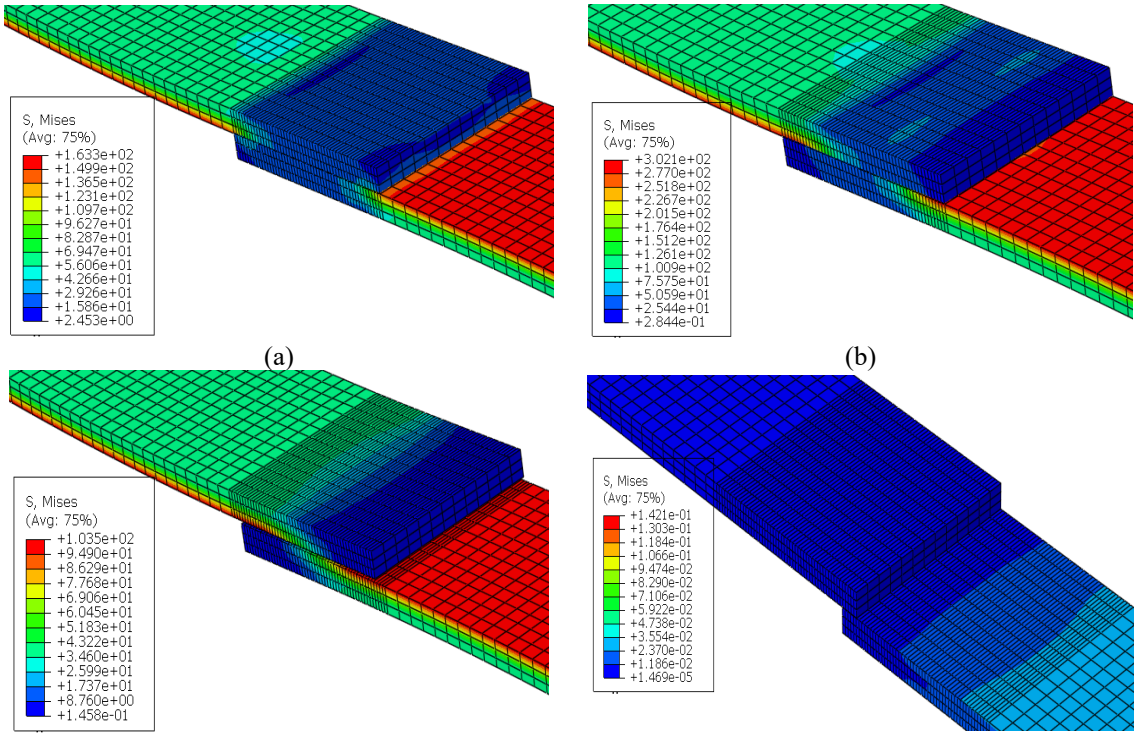

Figure 6. Von Mises stress distribution (MPa) in the single-lap joint during the damage development process: (a) before damage (δ = 2.5 mm), (b) damage initiation (δ = 2.85 mm), (c) damage evolution (δ = 3.3 mm) and (d) after damage (δ = 4.0 mm)

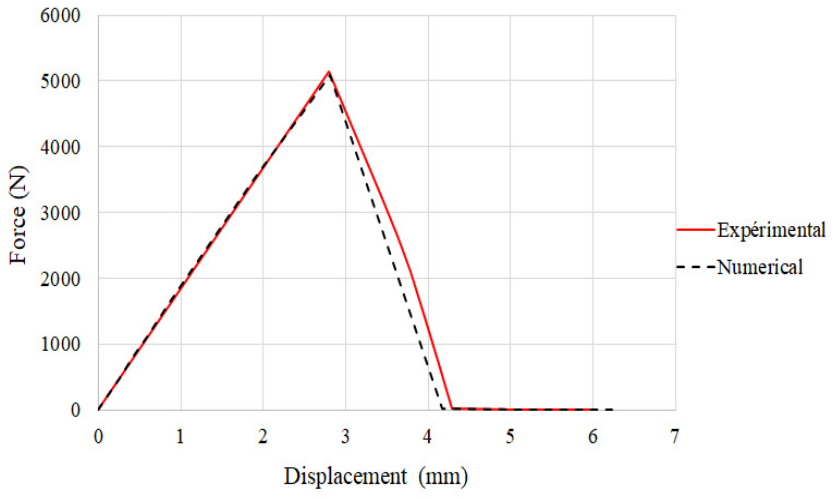

Figure 7. Comparison of numerical and experimental force-displacement curves for a single-lap joint with Adekit A-140 adhesive

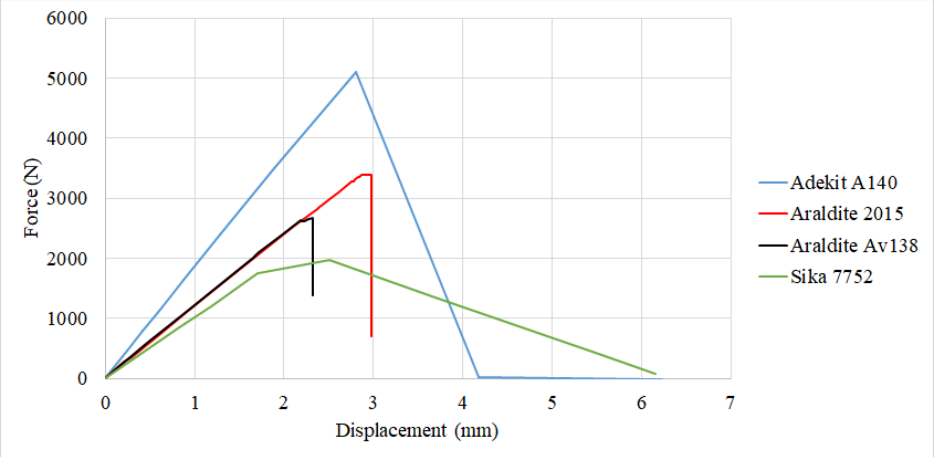

Figure 8. Force-Displacement curves for different adhesives: Adekit A140 - Araldite AV138 - Araldite 2015 - Sikaforce 7752

The force increases linearly with displacement until reaching approximately 5000 N at a displacement of 2.85 mm, corresponding to an almost elastic response of the joint. The joint geometry induces a non-uniform stress distribution, resulting in stress concentrations at the overlap ends, where the combined action of normal and shear stresses promotes mixed-mode loading and accelerates damage initiation and failure. Consequently, once damage initiates, the deformation rapidly localizes, leading to premature failure of the bonded joint.

5.2 Damage and failure of single-lap joints with different adhesives

Fig. 8 shows the force-displacement curves for different adhesive joints (Adekit-A140, Araldite AV138, Araldite 2015, and Sikaforce 7752), where Araldite AV138 and Araldite 2015 share the same chemical composition.

By comparing the various curves, it is evident that the joint with Adekit A140 is the strongest, reaching a maximum failure force of 5000 N. Conversely, Sikaforce 7752 is the weakest, with a maximum failure force of 2031 N. Additionally, the joint bonded with Araldite 2015 exhibits greater joint toughness compared to Araldite AV138. Furthermore, the joint bonded with Sikaforce 7752 shows a larger plastic deformation zone than the other adhesives. Both adhesives, Araldite 2015 and Araldite AV138, exhibit a similar initial linear response, indicating comparable elastic stiffness. However, Araldite 2015 shows superior mechanical performance, characterized by a failure force approximately 15% higher and a joint displacement at failure about 45% greater than that of Araldite AV138. This behavior highlights the enhanced load-carrying capacity and ductility of joints bonded with Araldite 2015.

5.3 Study of the Bi-adhesive single-lap joint using two adhesives (Araldite AV138 and Araldite 2015)

The effectiveness of the bonded joint using two adhesives with the same chemical composition, Araldite AV138 and Araldite 2015, was studied. The bi-adhesive configuration was selected due

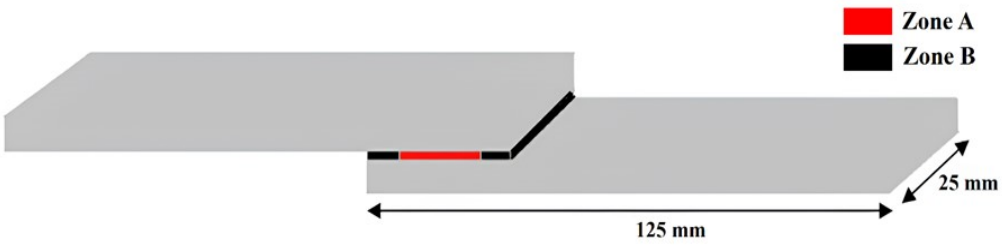

Figure 9. Schematic representation of a Bi-Adhesive Single-Lap Joint

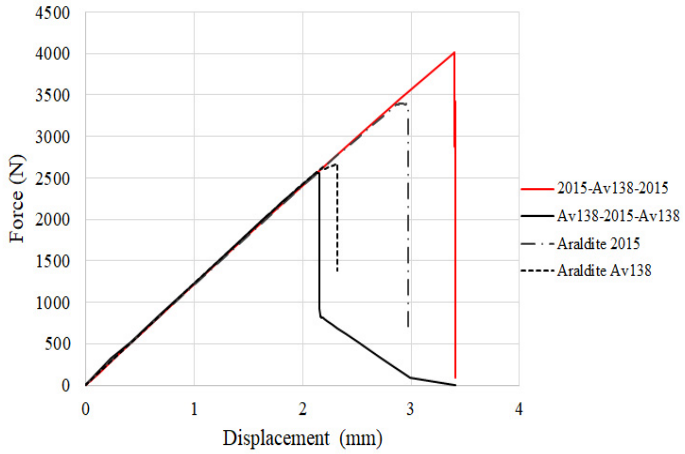

Figure 10. Force-Displacement Curves of Bi-Adhesive Joints Using Araldite 2015 and Araldite AV138

to the strong contrast in mechanical behavior between Araldite AV138 and Araldite 2015. This pronounced contrast makes this pair particularly suitable for investigating the effectiveness of the bi-adhesive concept. The objective of this study is to activate the core of the joint by varying the placement of the stiffer adhesive, either at the ends or in the middle of the joint. Fig. 9 illustrates a single-lap joint with the application of two adhesives: the central zone ('A'), 10 mm in length, represents adhesive 'A', while the outer zones ('B'), each 7.5 mm long, represent adhesive 'B'.

Fig. 10 presents a comparison between bonded joints with a single adhesive and bi-adhesive joints using Araldite AV138 and Araldite 2015. In this study, the placement of the two adhesives was varied, either at the core or at the ends of the joint. When Araldite 2015 was placed at the core (zone 'A'), the force increased until reaching a maximum value of 2650 N, followed by a gradual decrease until complete joint failure. However, positioning Araldite AV138 (the stiffer adhesive) at the core provided greater reinforcement to this region, leading to an overall strength improvement of 37.5%. This improvement is attributed to the contribution of the adhesive stiffness at the core of the joint. Placing the stiffer adhesive in the middle acts as a barrier to crack propagation, thereby increasing the joint strength. In contrast, when the less stiff adhesive is placed at the center, the crack propagates freely without being hindered.

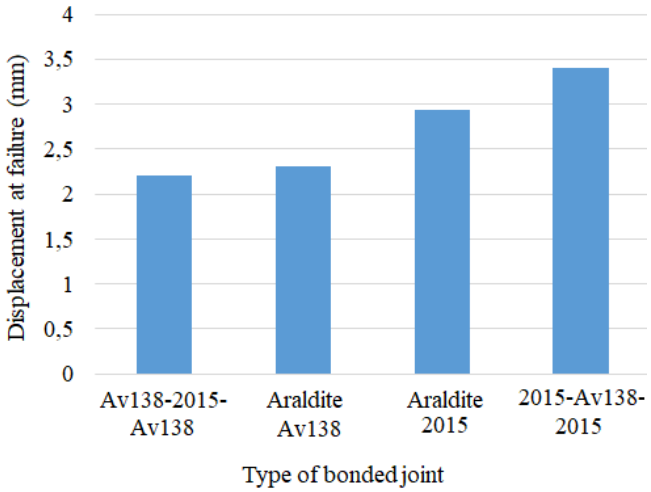

Figure 11. Histograms of displacements at the maximum failure force for the different types of joints. (Araldite Av138, Araldite 2015, Av138-2015-Av138 and 2015-Av138-2015)

Fig. 11 presents the displacements at maximum failure force for the different types of joints (Araldite AV138, Araldite 2015, AV138–2015–AV138, and 2015–AV138–2015). The results clearly show that the bi-adhesive joint with Araldite AV138 (the stiffest adhesive) placed at the center requires a greater imposed displacement to reach the maximum failure load compared to the other joints. This improvement is attributed to the contribution of the joint core in reinforcing the overall strength.

5.4 The energy absorption

The energy absorption (EA) was calculated from the area under the force–displacement curves for each bi-adhesive joint. A comparison of EA for the different joint configurations is presented in Fig. 12. This comparison shows that most of the strength of the bi-adhesive joint comes from the stiffer adhesive placed at the core. Conversely, placing the more flexible adhesive (Araldite 2015) in the middle reduces the energy absorption capacity of the joint. Therefore, positioning the stiffer adhesive in the center improves the energy absorption, with an increase of approximately 53% compared to the (Av138–2015–Av138) configuration, and about 26% compared to the joint bonded entirely with Araldite 2015.

5.5. Study of joint overlap length variation with the application of two adhesives: Araldite AV138 and Araldite 2015

A variation in the length of Araldite 2015 at the ends was applied with values of 5 mm, 7.5 mm, and 10 mm to observe the joint behavior as the overlap length of the bi-adhesive joint changed (Fig. 13).

By varying the length of Araldite 2015 at the ends of the joints, Fig. 13 shows that the force increases with the imposed displacement. The different curves exhibit similar behavior, with the joints containing 7.5 mm and 5 mm of Araldite 2015 at the ends being almost indistinguishable.

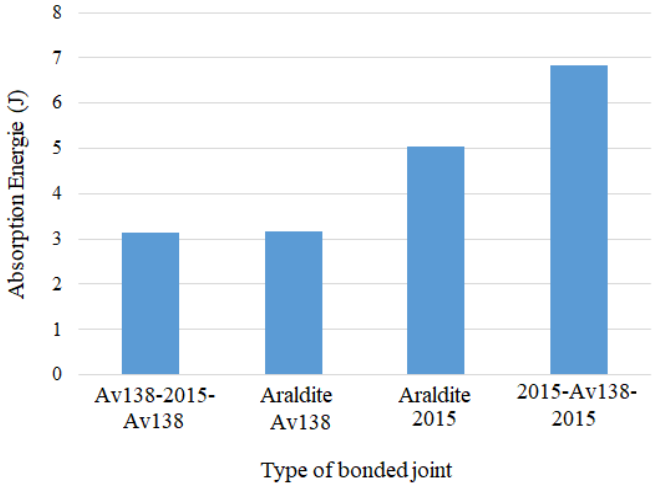

Figure 12. Variation of energy absorption for the different joints (Araldite Av138, Araldite 2015, Av138-2015-Av138 and 2015-Av138-2015)

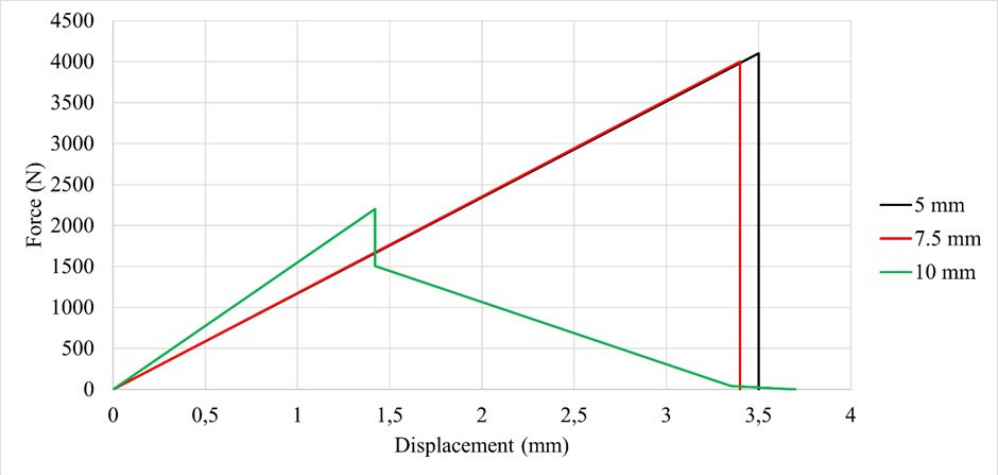

Figure 13. Force-Displacement curves of bi-adhesive joints with different overlap lengths using Araldite 2015/AV138/2015

To reach joint failure, a larger imposed displacement is required for the joint containing 60% of Araldite AV138 compared to those with 40% and 20%, respectively. In terms of strength, the bonded joint with 5 mm adhesive length at the ends shows an improvement of 5% and 53.5% compared to the joints with 7.5 mm and 10 mm, respectively.

6. Conclusions

The objective of this study was to simulate, using finite element analysis, the damage and failure of single-lap bonded joints under uniaxial loading with various adhesives: Adekit A140, Araldite 2015, Araldite AV138, and Sikaforce 7752.

A cohesive zone model (CZM) was used to analyze crack propagation. The cohesive zone was defined using cohesive elements governed by a bilinear traction–separation law.

In the first part, a comparison was conducted between the numerical results and the experimental data Ezzine et al. [25], showing excellent agreement, as the curves nearly overlap. The aim was to develop a finite element model incorporating CZM to simulate failure behavior due to crack propagation in a shear test of a bonded joint using the adhesive Adekit A140. This validated model was subsequently used throughout the remainder of the study.

In the second part, bi-adhesive joints were numerically analyzed using CZM. The goal was to investigate joint behavior by varying the placement of the stiffer adhesive (Araldite AV138), either at the ends or at the center, in order to activate the joint core, which is often inactive. This configuration proved effective when the stiffer adhesive was placed at the center, resulting in a 37.5% improvement in strength compared to the configuration where Araldite 2015 was placed in the core.

Additionally, to further characterize joint performance, we analyzed the displacement at maximum failure force and the energy absorption (EA) derived from the area under the force–displacement curves. The results demonstrated that the bi-adhesive joint with the stiff adhesive (Araldite AV138) placed at the center not only achieved the highest displacement at failure but also exhibited the greatest energy absorption. Specifically, this configuration showed an increase in EA of approximately 53% compared to the AV138–2015–AV138 joint, and 26% compared to the joint bonded entirely with Araldite 2015. These findings highlight the effectiveness of combining adhesives with contrasting mechanical properties to enhance both strength and toughness of bonded joints.

The third part of the work focused on the effect of varying the overlap length of the stiffer adhesive (Araldite AV138) in the bi-adhesive joint. The best-performing configuration among the tested cases was observed when Araldite AV138 covered 60% of the total overlap length, yielding an increase in joint strength ranging from 5% to 46% compared to configurations with 40% and 20% coverage, respectively. Building upon these findings, future works and perspectives include conducting a more extensive experimental study to further validate and generalize the results, as well as implementing artificial intelligence (AI) techniques to predict damage and optimize the design of adhesive joints, aiming to improve their mechanical performance and energy absorption.

Acknowledgments

The authors would like to express their sincere gratitude to the Laboratory of Mechanics and Physics of Materials (LMPM) at Djillali Liabes University for their valuable support. The authors also acknowledge the General Directorate of Scientific Research and Technological Development (DGRSDT).

References

1. Sassi, S., Tarfaoui, M., Yahia, H.B. (2018). An investigation of in-plane dynamic behavior of adhesively-bonded composite joints under dynamic compression at high strain rate. Composite Structures, 191, 168-179. https://doi.org/10.1016/j.compstruct.2018.02.057.
2. Liu, R., Zhang, P., Shen, G., Li, Q., Liu, S., Zhou, W. (2023). Acoustic emission study on damage

mechanism of composite materials repaired with bi-adhesive and damage classification model. Journal of Adhesion Science and Technology, 38(10), 1718-1737. https://doi.org/10.1080/01694243.2023.2270731.

3. Karachalios, E.F., Adams, R.D., daSilva, L.F.M. (2013). Single lap joints loaded in tension with high strength steel adherends. International Journal of Adhesion and Adhesives, 43, 81-95. https://doi.org/10.1016/j.ijadhadh.2013.01.017.
4. Da Silva, L.F., Adams, R.D. (2007). Techniques to reduce the peel stresses in adhesive joints with composites. International Journal of Adhesion and Adhesives, 27(3), 227-235. https://doi.org/10.1016/j.ijadhadh.2006.04.001.
5. Özer, H., Öz, Ö. (2012). Three dimensional finite element analysis of bi-adhesively bonded double lap joint. International Journal of Adhesion and Adhesives, 37, 50-55. https://doi.org/10.1016/j.ijadhadh.2012.01.016.
6. da Silva, L.F.M., Lopes, M.J.C.Q. (2009). Joint strength optimization by the mixed-adhesive technique. International Journal of Adhesion and Adhesives, 29, 509-514. https://doi.org/10.1016/j.ijadhadh.2008.09.009.
7. Pires, I., Quintino, L., Miranda, R.M. (2006). Numerical simulation of mono- and bi-adhesive aluminium lap joints. Journal of Adhesion Science and Technology, 20(1), 19-36. https://doi.org/10.1163/156856106775212387.
8. Öz Ö., Özer H. (2014). On the von Mises elastic stress evaluations in the bi-adhesive single lap joint: a numerical and analytical study. Journal of Adhesion Science and Technology, 28, 2133-2153. https://doi.org/10.1080/01694243.2014.948110.
9. Bellali, M.A., Serier, B., Mokhtari, M., Campilho, R.D.S.G., Lebon, F., Fekirini, H. (2021). XFEM and CZM modeling to predict the repair damage by composite patch of aircraft structures: debonding parameters. Composite Structures, 266, 113805. https://doi.org/10.1016/j.compstruct.2021.113805.
10. Sliwa-Wieczorek, K., Zaj, B. (2021). Rigid and flexible double shear lap adhesive jointat elevated temperature—an experimental study. Polymers, 13(17), 2873. https://doi.org/10.3390/polym13172873.
11. Völkersen, O. (1938). Die Nietkraftverteilung in Zugbeanspruchten Neitverbeindun- gen mit Konstanten Laschequerschnitten. Die Luftfahrtforschung, 15, 41-47.
12. Baghdadi, M. (2019). Assessing composite patch repair efficiency in thick and high elastic modulus structures. Advances in Aircraft and Spacecraft Science, 11(3), 215-230. https://doi.org/10.12989/aas.2024.11.3.215.
13. Rudawska, A. (2019). Bonding technology. Surface Treatment in Bonding Technology, 7-46. https://doi.org/10.1016/B978-0-12-817010-6.00002-3.
14. Sankar, H.R., Adamvalli, M., Kulkarni, P.P., Parameswaran, V. (2015). Dynamic strength of single lap joints with similar and dissimilar adherends. International Journal of Adhesion and Adhesives, 56, 46-52. https://doi.org/10.1016/B978-0-12-817010-6.00002-3.
15. Dhilipkumar, T., Rajesh, M. (2021). Enhancing shear strength and structural stiffness of composite joint with carbon nanotube reinforced adhesive through co-bonding technique. Journal of Adhesion Science and Technology, 36(19), 2143-2157. https://doi.org/10.1080/01694243.2021.2002066.
16. Papanicolaou, G.C., Karagiannis, D., Kousiatza, C., Kontaxis, L.C., Portan, D.V. (2022). Flexural behavior of single-lap joints of similar and dissimilar adherends. Journal of Adhesion Science and Technology, 37(4), 624-648. https://doi.org/10.1080/01694243.2022.2035050.
17. Benzaama, A., Mokhtari, M., Ahmed-Bouziane, N.E.I., Abdelouahed, E., Habib, B., Ghermaoui, I.M. A., Aliane, I. (2023). Using a UMM-XFEM technics to predict the damage in CFRP bi-graded with glass-epoxy materials of notched plate under quasi-static loading. Mechanics of Advanced Materials and Structures, 31(25), 7367-7385. https://doi.org/10.1080/15376494.2023.2244958.
18. Ghermaoui, I.M.A., Mokhtari, M., Benzaama, H., Elamine, A. (2023). Using FGM concept and combined of XFEM-CZM technics to predict the damage in carbon/carbon-epoxy graded composites. Mechanics of Advanced Materials and Structures, 31(25), 7526-7544. https://doi.org/10.1080/15376494.2023.2245830.
19. Kouno, Y., Takeda, N. (2019). Estimation of fracture behavior of CFRP/CFRP adhesively bonded joints

under mixed-mode conditions using a cohesive zone model. Journal of Adhesion Science and Technology, 33(6), 623-637. https://doi.org/10.1080/01694243.2024.2348244.

20. Ezzine, M.C., Amiri, A., Tarfaoui, M., Madani, K. (2018). Damage of bonded, riveted and hybrid (bonded/riveted) joints, experimental and numerical study using CZM and XFEM methods. Advances in Aircraft and Spacecraft Science, 5(5), 595-613. https://doi.org/10.12989/aas.2018.5.5.595.
21. Da Silva, L.F.M., Campilho, R.D.S.G. (2011). Advances in numerical modelling of adhesive joints. Heidel berg: Springer.
22. Lopes, V.H.P., Campilho, R.D.S.G., Nóvoa, P.J.R.O., Rocha, R.J.B., Sánchez-Arce, I.J. (2022). Experimental and cohesive zone modelling study on composite joining by co-curing and adhesive bonding for sheet moulding compound or carbon-fibre prepreg laminates. Journal of Adhesion Science and Technology, 37(9), 1593-1613. https://doi.org/10.1080/01694243.2022.2081446.
23. Crocombe, A., Hua, Y., Loh, W., Wahab, M., Ashcroft, I. (2006). Predicting the residual strength for environmentally degraded adhesive lap joints. International Journal of Adhesion and Adhesives, 26, 325-336. https://doi.org/10.1016/j.ijadhadh.2005.04.003.
24. Kouno, Y., Imanaka, M., Hino, R., Omiya, M., Yoshida, F. (2024). Estimation of fracture behavior of CFRP/CFRP adhesively bonded joints under mixed-mode conditions using a cohesive zone model. Journal of Adhesion Science and Technology, 38(19), 3618-3635. https://doi.org/10.1080/01694243.2024.2348244.
25. Ezzine, M.C., Amiri, A., Tarfaoui, M. (2018). Experimental and numerical investigation of the fracture behaviour of adhesive shear tests single lap joints. Journal of the Brazilian Society of Mechanical Sciences and Engineering, 40, 382. https://doi.org/10.1007/s40430-018-1303-5.
26. Moreira, R.D.F., Moura, M de, Silva, F.G.A., Ramirez, F.M.G., Rodrigues, J.S. (2020). Mixed-mode I+II fracture characterisation of composite bonded joints. Journal of Adhesion Science and Technology, 34, 1385-1398. https://doi.org/10.1080/01694243.2019.1708645.
27. Santos, M.A.S., Campilho, RD.S.G. (2017). Mixed-mode fracture analysis of composite bonded joints considering adhesives of different ductility. International Journal of Fracture, 207(1), 55-71. https://doi.org/10.1007/s10704-017-0219-x.
28. Li, G., Li, C. (2014). Linking bilinear traction law parameters to cohesive zone length for laminated composites and bonded joints. Advances in Aircraft and Spacecraft Science, 1(2), https://doi.org/10.12989/aas.2014.1.2.177.
29. Camanho, P.P., Dávila, C.G. (2002). Mixed-mode decohesion finite elements for the simulation of delamination in composite materials. National Aeronautics and Space Administration, NASA/TM-2002-211737.
30. Campilho, R.D.S.G., de Moura, M.F.S.F., Ramantani, D.A., Morais, J.J.L., Domingues, J.J.M.S. (2009). Buckling behaviour of carbon–epoxy adhesively-bonded scarf repairs. Journal of Adhesion Science and Technology, 23(10-11), 1493-1513. https://doi.org/10.1163/156856109X433045.
31. Benzeggagh, M.L., Kenane, M. (1996). Measurement of mixed-mode delamination fracture toughness of unidirectional glass/epoxy composites with mixed-mode bending apparatus. Composites Science and Technology, 56(4), 439-449. https://doi.org/10.1016/0266-3538(96)00005-x.